SEVENTH FRAMEWORK PROGRAMME

THEME FP7-ICT-2009-C

Instrument	STREP
Project no.	244068
Project acronym	**CROSSTRAP**
Project title	**C**oherently-enhanced **R**aman **O**ne-beam **S**tandoff **S**pectroscopic **TR**acing of **A**irborne **P**ollutants

Deliverable D2.3

Standoff SRS

Due date of deliverable	month 40
Actual submission date	24/06/2013
Start date of project	01/02/2010
Duration of the project	40 months
Organization name of lead contractor for this deliverable	**POLIMI**
Dissemination Level	public

INDEX

1_ INTRODUCTION

In this deliverable we aim at achieving the main goal of the CROSSTRAP project: demonstration of remote sensing using a coherent beam propagating backward from the interrogated region to the observer. This achievement is based on several prerequisites: identification of a suitable coherent detection approach providing a backward propagating signal; development of the necessary laser system; setup of a detection apparatus providing the required sensitivity.

Section 2 reviews the different possible approaches for coherent backward detection and presents the one chosen in this project: stimulated Raman scattering (SRS) using a backward propagating atmospheric laser as a probe.

Section 3 presents the preliminary results on backward SRS using two narrowband, synchronized counter-propagating pulses, one of which mimics the atmospheric laser. This study allows to evaluate the parameters necessary for a true standoff detection.

Section 4 presents the concept and the parameters of the free-space nitrogen laser driven by a femtosecond filament. Generation of population inversion in the filament is accomplished using a high-energy mid-IR driver laser, the characteristics of which are here reported.

Section 5 describes the architecture of a standoff SRS setup based on a backward propagating atmospheric laser.

Section 6 presents a system characterization and the first results of backward SRS using a filament laser as a probe, which is the fundamental milestone of CROSSTRAP.

Finally section 7 presents some preliminary work towards broadening the spectrum and shaping the temporal profile of the mid-IR pulses, aimed at optimizing the population inversion in the filament and the performance of the atmospheric laser.

2_ Discussion of coherent backward detection approaches

Many applications in environmental science and homeland security call for standoff identification of airborne pollutants with the highest possible sensitivity and chemical specificity. Optical techniques such as Light Detection and Ranging (LIDAR) and differential LIDAR (DIAL) offer powerful tools for the remote sensing of trace gases and aerosols (including hazardous species) in the atmosphere [1, 2], proving useful for environment protection, meteorology, geosciences, archeology, forestry, agriculture, and homeland security. LIDAR systems based on Raman scattering allow a fingerprinting of molecules using their unique vibrational spectral signatures, providing a high degree of chemical specificity [3]. Rapidly progressing coherent LIDAR technologies [2] push the frontiers of advanced atmospheric research, enabling high-sensitivity and high-resolution atmospheric wind profiling. The success of heterodyne detection as a cornerstone concept of the existing coherent LIDAR approaches inspires a broader use of coherent processes and methods, motivating the development of optical remote sensing strategies where coherence is not limited to the detection of the backscattered signal return, but is used to provide a highly directional backward optical signal through coherent Raman scattering [4–7], thus enhancing the sensitivity and selectivity of standoff detection. However, with fully ground-based laser systems, delivering only forward beams, generation of coherent backward signals is prohibited by momentum conservation, manifested as the phase-matching condition in coherent wave mixing. The search for the solutions to this fundamental problem is ongoing, with the latest theoretical proposals including the use of electromagnetically induced coherent backscattering [8], plasma-assisted backscattering [9], as well as combinations of laser and radar methods [10]. The recent discovery of remotely pumped lasing in the atmosphere, using atomic oxygen [11] or molecular nitrogen [12], provides a unique remote source of coherent backward radiation. It is due to this discovery that the long-standing challenge of backward coherent optical signal generation, needed to enhance sensitivity and selectivity of coherent remote sensing, can now be experimentally confronted.

The principle scheme of a remote sensing system based on an atmospheric laser, which lies at the hearth of the CROSSTRAP project, is shown in Fig. 1. The observer fires a first powerful ultrashort laser pulse (Laser 1) which, focused in the atmosphere, generates a filament, inside which a population inversion and laser action are created. The atmospheric laser emits a pulse which propagates back towards the observer. At the same time the observer fires a second laser pulse (Laser 2), synchronized and delayed with respect to Laser 1 and with a suitable frequency detuning from the atmospheric laser. The atmospheric laser pulse and Laser 2 are temporally and spatially overlapped in a certain region of space, where the pollutant to be detected is present. The nonlinear interaction between the two pulses is mediated by the interrogated molecules, whose spectral signature will be imprinted on the atmospheric laser pulse, which is finally detected by the observer.

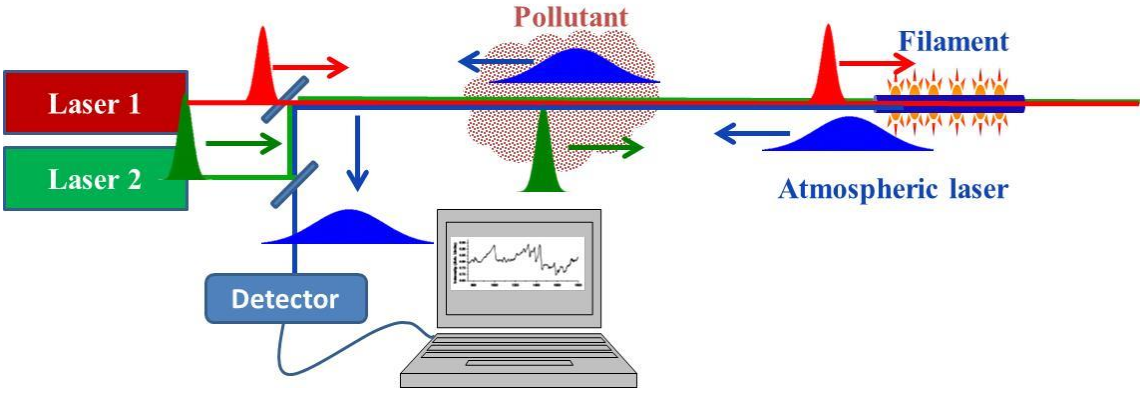

Fig. 1. *Principle scheme of the remote sensing experiment using a backward propagating atmospheric laser.*

Several nonlinear optical processes can be used for the purpose of sensing. Two-photon absorption (i.e. simultaneous absorption of one photon from laser 2 and one photon from the atmospheric laser to reach an electronic transition) is inherently phase-matched, but does not have a high molecular specificity, as electronic transitions are typically broad and featureless. Coherent Raman scattering (CRS) techniques, on the other hand, provide a high degree of molecular specificity and allow vibrational fingerprinting. CRS requires simultaneous excitation of the molecular specimen with two beams, the pump (at frequency ω_P) and the Stokes (at frequency ω_S) with frequency detuning matching a molecular vibration, $\omega_P-\omega_S=\Omega$. Coherent antiStokes Raman scattering (CARS) detects the signal at the antiStokes frequency, $\omega_{aS}=2\omega_P-\omega_S$. Stimulated Raman scattering (SRS) is a pump-probe technique, detecting the stimulated Raman gain (SRG) of the Stokes or the stimulated Raman loss (SRL) of the pump. For the purpose of remote sensing, SRS offers the following important advantages with respect to CARS:

(i) it is inherently phase-matched, thus allowing the implementation of a backward interaction geometry, which would be impossible using CARS due to wavevector mismatch [7];

(ii) it is free from the non-resonant background originated by the electronic contributions to the third-order nonlinear susceptibility [13, 14];

(iii) its signal scales linearly with the number of probed molecular oscillators, thus allowing the detection of relatively low-concentration specimens.

The main experimental challenge of SRS resides in the difficulty to measure the weak SRG/SRL sitting on top of an intense (possibly noisy) Stokes/pump pulse. For an SRS process, in the weak signal and monochromatic plane wave limits, one can write:

$$\Delta I_p \propto -\mathrm{Im}\left(\chi^{(3)}\right) I_p I_S L$$

$$\Delta I_S \propto +\mathrm{Im}\left(\chi^{(3)}\right) I_p I_S L$$

where I_P and I_S are the pump and Stokes intensities respectively, L is the interaction length and $\chi^{(3)}$ is the nonlinear Raman susceptibility of the transition under study. One can thus measure either the SRG of the Stokes beam:

$$SRG = \frac{\Delta I_S}{I_S} \propto +\mathrm{Im}\left(\chi^{(3)}\right) I_p L$$

or the SRL of the pump beam:

$$SRL = \frac{\Delta I_p}{I_p} \propto -\mathrm{Im}\left(\chi^{(3)}\right) I_S L$$

It is apparent that the pump and Stokes beams are fully interchangeable. It is thus convenient to use the more intense beam to induce a large stimulated signal and measure the intensity variations of the weaker "probe" beam, detected either as SRG or as SRL. For a given value of $\chi^{(3)}$ (which depends on substance to be detected and concentration), the two parameters that determine the strength of the SRS signal are the peak intensity of the pump (Stokes) pulse $I_p(I_S)$ and the interaction length L. For a given available pulse energy, the peak intensity scales inversely with pulse duration, so that shorter pulses give higher SRS signals; on the other hand, the pulse bandwidth should not exceed the width of the probed manifold of rotovibrational Raman lines, typically on the order of a few cm^{-1}. This dictates optimum pulsewidths ranging from a few to a few tens of picoseconds for the "stimulating" pulse (which can be either pump or Stokes according to the configuration). The sensing pulse, on the other hand, can have a narrower bandwidth, since its peak power does not affect the SRG/SRL. According to the scheme of Fig. 1, the atmospheric laser can thus play the role of a "probe" or sensing pulse, while an intense, picosecond long "stimulating pulse" will be generated by a ground-based laser system, synchronized with the laser driving the filament. In the next paragraph we will present one by one the logical steps leading to the successful demonstration of backward SRS registered with a filament laser.

3_ Review of preliminary backward SRS experiments

As an intermediate goal toward employing an atmospheric 337-nm N_2 laser for remote sensing, we first experimentally and theoretically investigated a prototype for backward SRS in air. The experimental approach is based on a laser system from which we derive narrowband UV pulses, imitating the N_2 laser emission from a filament and acting as Stokes pulses, and synchronized tunable narrowband UV pump pulses [15]. The system allows us to extrapolate the laser parameters required for a real remote sensing experiment.

The system starts with a 10 kHz Yb:KGW chirped pulse amplifier (CPA) (Pharos, Light Conversion) generating 400 μJ, 280 fs pulses centred at 1024 nm fundamental frequency. The system drives a second-harmonic-pumped optical parametric amplifier (OPA), producing 40 μJ, 200 fs pulses tunable between 620 and 700 nm. The OPA is seeded by a white light continuum, generated in a 6 mm long undoped YAG crystal, which is further amplified in two OPA stages based on 15 mm long Type I lithium triborate (LBO) crystals. The tunability of the OPA on the short wavelength side is limited by the absorption of the idler pulses in the LBO crystals. The OPA pulses are sent to a spectral compressor generating UV pulses (310-350 nm) serving as a tunable Raman pump. With a 20-mm-long

β-barium borate (BBO) crystal we obtain UV pulse energies from 2.5 to 10 μJ in the 310-340 nm wavelength range with linewidths of 30-40 cm^{-1}.

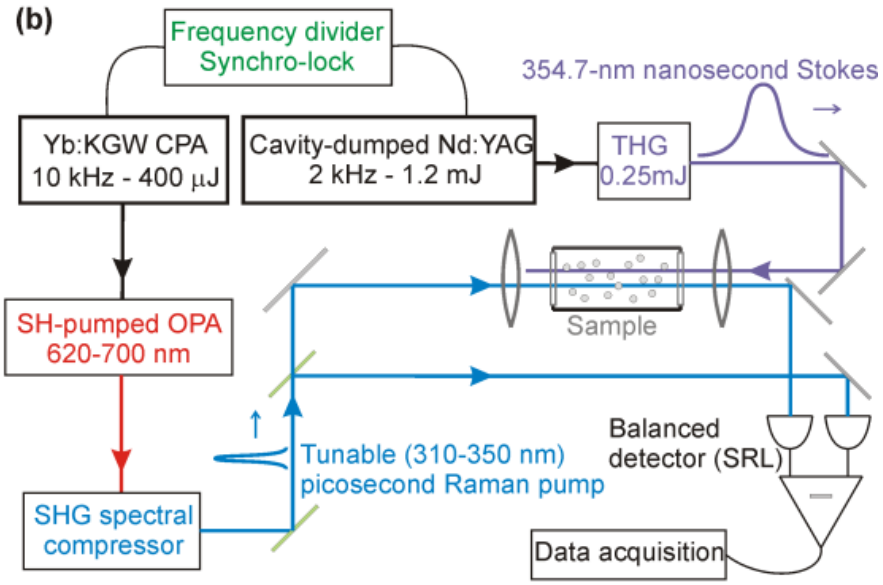

Fig. 2. *Setup of the proof-of-principle backward SRS experiment with picosecond pump and nanosecond Stokes pulses.*

The Yb:KGW laser is electronically synchronized with a home-built Q-switched cavity-dumped Nd:YAG laser, generating 1.2 mJ, sub-10 ns pulses at the repetition rate of 2 kHz, with rms energy stability of 5.5 %. These rather high energy fluctuations are characteristic of Q-switched cavity-dumped lasers where pulse generation starts from noise. The output of the Nd:YAG laser is frequency-tripled by in-line generation of the second harmonic and subsequent sum-frequency-generation with the 1064-nm pulse in 15 mm long Type I and Type II LBO crystals respectively, resulting in 250 μJ, 4-ns pulses at 355 nm. In order to increase the spatial beam quality, the 355-nm beam is apertured by a pair of irises, which results in a Stokes pulse energy of 135 μJ. The delay between pump and Stokes pulses is tuned electronically with the precision of 400 ps, which is determined by the time jitter of the cavity-dumped nanosecond pulses. Given the substantially larger energy of the Stokes pulse, we prefer in this setup to detect the SRL signal of the weaker pump. The Stokes is directly modulated dividing by 5 the clock signal derived from the Yb:KGW system and thus running the cavity-dumped Nd:YAG laser at 2 kHz.

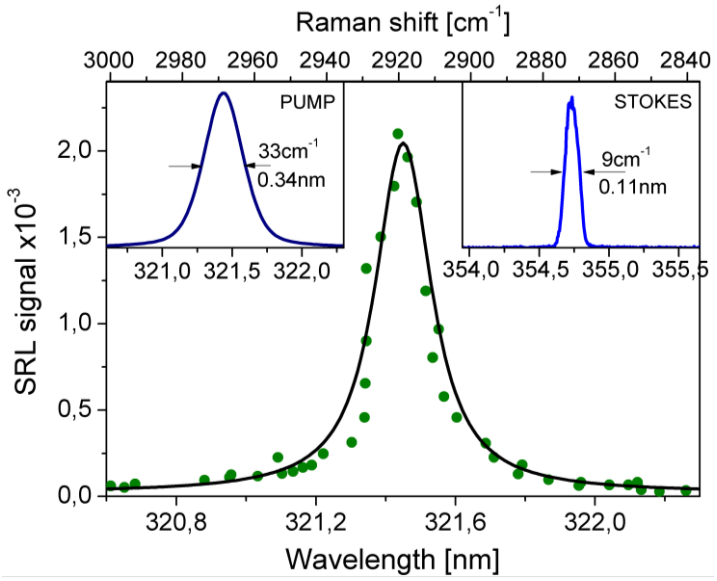

Fig. 3. *Spectrum of CH_4 (dots) and its theoretical fit (solid line) in the case of 5 bar pressure and 135-μJ Stokes energy. In the insets the spectra of Stokes and pump as measured with the spectrometers having respectively spectral resolution of 4 cm^{-1} and 20 cm^{-1} are given.*

We first performed backward SRS experiments in methane, contained in a pressurized cell. Figure 3 shows the SRL signal obtained when tuning the pump/Stokes frequency difference around the methane resonance at a pressure of 5 bar. One observes a strong peak around the central frequency of 2915 cm^{-1}, corresponding to the ν_1 band (symmetric CH stretching mode). The spectral response has a width of 17 cm^{-1} FWHM which is limited, as confirmed by our simulations (the solid line in Fig. 3), by the bandwidth of ps pump pulses. The SRL signal, with a maximum value of 2×10^{-3}, was found to scale linearly with the pump intensity.

Based on these results, we are now in a position to extrapolate the laser parameters required for a true standoff sensing based on backward SRS from an atmospheric laser and to design a system accordingly. Using a forward UV pump, provided by a ground-based laser, and a backward probe from a filamentation-assisted nitrogen laser in the atmosphere. In the regime of interest, the SRG/SRL signal scales with the product $G = gI_pL_{eff}$, where $g \propto d\sigma/d\Omega$ is the Raman gain coefficient, I_p is the intensity of the pump pulse and L_{eff} is the effective interaction length. A filamentation-assisted N_2 laser in the atmosphere delivers coherent UV pulses at 337 nm with a typical pulse width of ≈1 ns [12]. With Stokes pulses of duration $\Delta\tau_p$ ≈ 20 ps, the temporal walk-off length of the pump and probe pulses is estimated as L_{temp} ≈ 15 cm. This large walk-off length is highly favorable for the standoff detection mode as it allows a strong enhancement of the SRS signal and enables the remote sensing of the atmosphere using loosely focused light beams.

4_ BACKWARD NITROGEN LASING FROM A FILAMENT

Because of the abundance of nitrogen in Earth's atmosphere, achieving nitrogen lasing via remote excitation would pave the way to many potential applications. In particular, a narrowband source of coherent, highly directional radiation would be ideal for highly selective and sensitive remote spectroscopy of the atmosphere. Filamentation of intense femtosecond pulses creates a plasma channel in which several chemical reactions take place, giving rise to a large variety of neutral and ionic species in rotationally, vibrationally, and electronically excited states. This may generate favorable conditions for population inversion and lasing between different electronic levels in N_2.

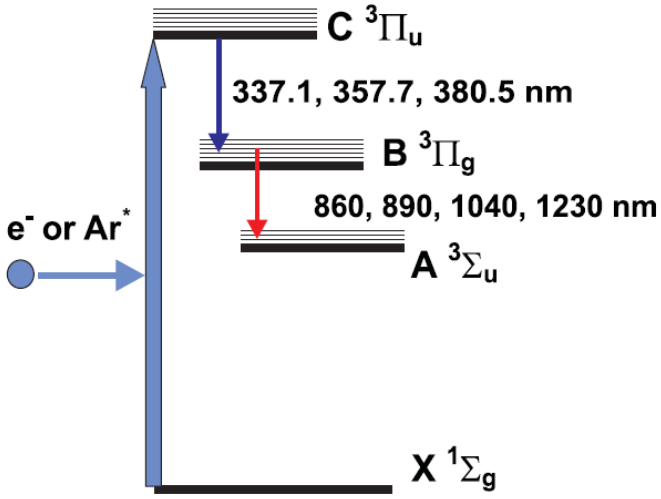

Fig. 4. *Energy levels scheme for a collisionally pumped N_2 laser.*

The energy levels scheme used in a collisionally pumped N_2 laser is reported in Fig. 4. Lasing occurs according to a three-level scheme in which the upper laser level, the C $^3\Pi_u$ triplet state, is populated by electron impact excitation from the singlet ground state X $^1\Sigma_g$. Laser action then can take place between the vibrational manifolds of the C $^3\Pi_u$ and the B $^3\Pi_g$ states. In a discharge pumped laser, one creates a plasma of hot electrons with kinetic energies around 15 eV, the peak of the excitation cross-section for the C $^3\Pi_u$ level. In a filament, it is not possible to control the electron temperature during the inversion build-up phase, as well as the duration of the plasma. To facilitate inversion, we play two tricks: i) used of a mid-IR (3.9 μm) driver pulse; ii) addition of Ar to the N_2 gas mixture. The use of a mid-IR driver, with respect to the standard Ti:sapphire wavelength (0.8 μm) brings with it several benefits: first of all the critical power for self-focusing scales as λ^2, allowing to put significantly higher powers (up to 250 GW) in a single filament. Then the ponderomotive energy of the electrons in the laser field, which also scales with λ^2, is considerably higher (E_p = 48 eV for a 3.9 μm driver vs. E_p = 2 eV for a 0.8 μm driver) allowing to reach significantly higher electron temperature in the discharge. The addition of Ar gas facilitates excitation of the C $^3\Pi_u$ upper laser level through a resonant excitation energy transfer mechanism (Bennett mechanism). First excited metastable atoms of argon are produced as a result of a

two-step kinetic process in the filament plasma involving three-body collisions $Ar^+ + 2Ar \rightarrow Ar_2^+ + Ar$ followed by dissociative recombination $Ar_2^+ + e \rightarrow Ar^*(4^3P_2) + Ar$. Excited state population in N_2 then occurs through the process $Ar^*(4^3P_2) + N_2 (X\ ^1\Sigma_g) \rightarrow Ar + N_2 (C\ ^3\Pi_u)$.

The atmospheric laser is driven by a high-power mid-infrared (mid-IR) optical parametric chirped pulse amplifier (OPCPA), providing 80-fs, 8-mJ pulses at a 20-Hz repetition rate at a wavelength of 3.9 μm [16]. Since this system is the key for the development of the standoff SRS setup presented in the following sections, it will be here briefly described.

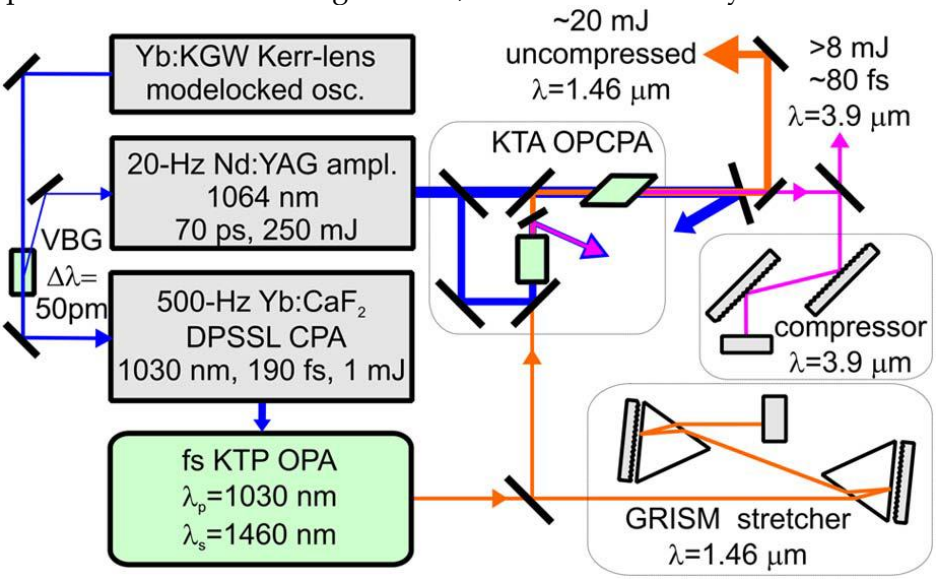

Fig. 5. *Layout of the 3.9 μm OPCPA system.*

The layout of the OPCPA is presented in Fig. 5. The front end of the system is a 190 fs $Yb:CaF_2$ CPA driving three cascades of a white-light seeded OPA based on KTP crystals, at the repetition rate of 0.5 kHz. The output energy in the signal wave after the last OPA stage is 65 μJ and provides the seed for the OPCPA. The pump laser for the OPCPA is a flash-lamp pumped Nd:YAG system based on a regenerative amplifier and two booster amplifiers, producing 70 ps pulses with energies above 250 mJ at 20 Hz. Both Yb and Nd pump lasers are optically synchronized by a common Yb:KGW seed oscillator. The OPCPA consists of two stages based on 10mm long KTA crystals. To reduce the risk of optical coating damage by mid-IR pulses, the final-stage crystal features uncoated Brewster cut faces that provide high transmission for p-polarized pump and idler waves. The OPCPA pulses at 3.9 μm are compressed with a grating pair, resulting in pulses with energy in excess of 8 mJ and nearly transform-limited 83 fs duration.

To drive the filament laser, the OPCPA beam is focused by a f = 2 m focusing lens into a 4-m-long gas cell with Brewster-angled input and output windows made of CaF_2. An uncoated CaF_2 plate is inserted into the input beam to enable characterization of backward emission from the filament. Below the lasing threshold, a well-known UV fluorescence spectrum of N_2 is observed from the gas cell [Fig. 6(a)]. At the input mid-IR pulse energy of 7 mJ, backward UV nitrogen lasing from the gas cell is observed at the nitrogen pressure

above 0.3 bar and the argon pressure above 3 bar. Lasing was achieved simultaneously for two lines at 337 and 357 nm [Fig. 6(b)], belonging to the second positive band of N_2. The threshold and efficiency of lasing as a function of partial pressures of nitrogen and argon in the gas mixture are summarized in Fig. 7. It can be seen that laser action takes place only for an argon pressure exceeding 3 bar [12]. At a fixed nitrogen pressure, the lasing efficiency increases with the increase of argon pressure and saturates at around 6 bar [Fig. 7(a)]. At a fixed argon pressure, first the lasing efficiency increases with the increase of nitrogen pressure and then drops after passing a broad maximum at around 1.7 bar [Fig. 7(b)].

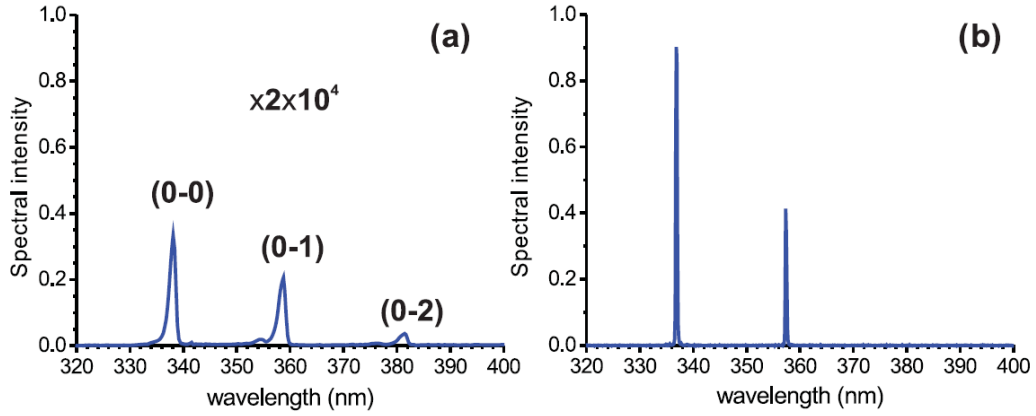

Fig. 6. *Spectra of (a) fluorescence from 1 bar of pure nitrogen and (b) lasing from the 1 bar of N_2 and 5 bars of Ar mixture.*

For the optimal mixture (1 bar N_2 and 5 bar Ar), the measured sum energy at 337 and 357 nm lines reached up to 3.5 μJ, corresponding to a 0.5% energy conversion efficiency from the mid-IR laser pulse to UV radiation. The temporal profiles of the N_2 laser pulses at 337 and 357 nm are presented in Fig. 7(a): lasing at 337 nm develops about a nanosecond earlier than at 357 nm and is emitted as a shorter subnanosecond pulse, whereas the duration of a 357-nm pulse is about 2 ns FWHM. The measured spatial beam profile is shown in Fig. 7(b) and has a roughly super-Gaussian shape. Low beam divergence of about 1.6 mrad was retrieved by measuring the beam profile as a function of the distance from the gas cell. Insertion of a 2-mm-thick CaF_2 parallel plate in the beam results in the appearance of clearly seen interference fringes [see inset on Fig. 7(b)], proving a high temporal coherence of the generated UV emission.

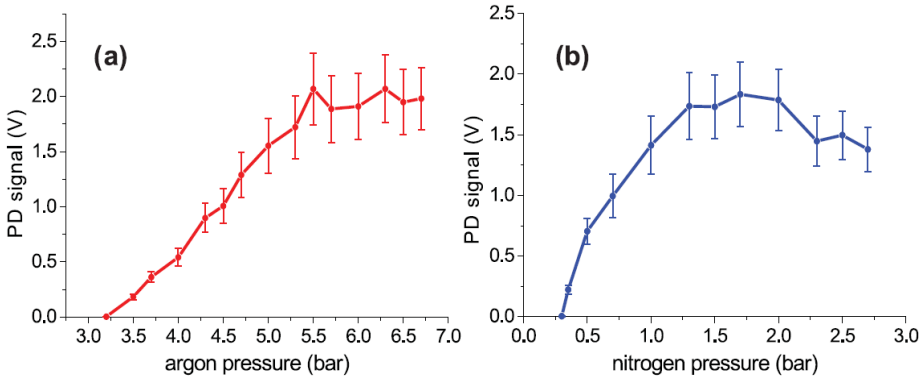

Fig. 7. *Dependence of the total lasing efficiency on (a) partial pressure of argon for fixed partial pressure of nitrogen 1 bar, and (b) partial pressure of nitrogen for fixed partial pressure of argon 5 bar.*

The parameters of the atmospheric nitrogen laser (pulse energy, pulse duration, spatial beam quality) are very well suited for the backward SRS sensing scheme presented in Fig. 1. We are therefore in a position to target the main goal of the CROSSTRAP project, i.e. the development of a coherent molecular detection scheme based on a backward propagating beam.

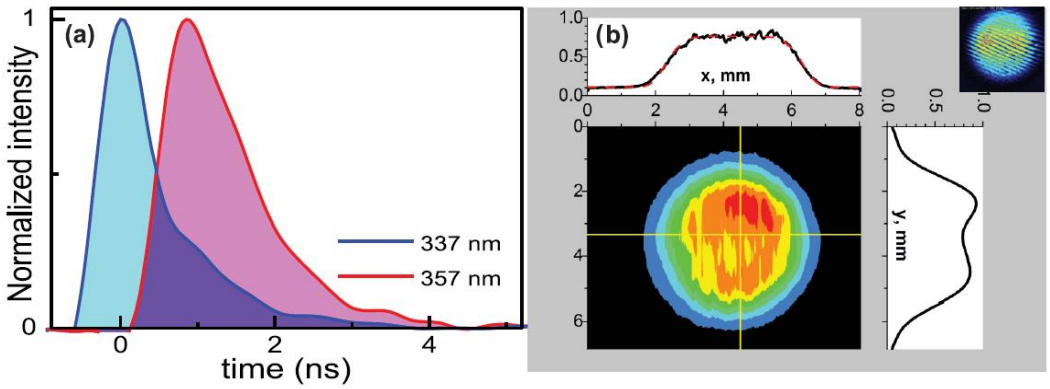

Fig. 8. *(a) Temporal profiles of the 337-nm (blue solid curve) and 357-nm (magenta dashed curve) laser pulses from the nitrogen-argon mixture. (b) The UV-lasing beam profile. The red dotted line shows a 6th-power super-Gaussian fit. Insert is a CCD image of interference in the beam from a 2-mm-thick CaF_2 parallel plate.*

5_ ARCHITECTURE OF A STAND-OFF SRS SETUP

The goal of this experiment, which is also the main objective of the CROSSTRAP project, is to achieve remote sensing of a gaseous sample via backward SRS with a Raman pump generated by lasing in the atmosphere. The conceptual architecture of the system is shown in Fig. 9: It requires the combination of the backward propagating, remotely pumped atmospheric N_2 laser (acting as a Raman pump beam) with a synchronized, narrowband tunable laser beam sent in the forward direction (acting as a Stokes beam). When the frequency difference between the pump and Stokes matches the Raman resonance of the

molecule to be detected, then the backward propagating Raman pump beam experiences SRL, enabling molecular fingerprinting. For spectral resolution, both pump and Stokes need to be narrowband and at least one needs to be broadly tunable in order to address different resonances. Since the atmospheric probe laser is already narrowband and at a fixed frequency (337 nm), we need to generate a tunable synchronized narrowband UV Stokes pulse. In our setup, the filament is initiated by a high-power mid-IR (4 μm) OPCPA driven by a femtosecond pump, while the tunable Stokes is obtained by nonlinear frequency conversion of the laser pulses generated by the same laser system that drives the mid-IR OPCPA.

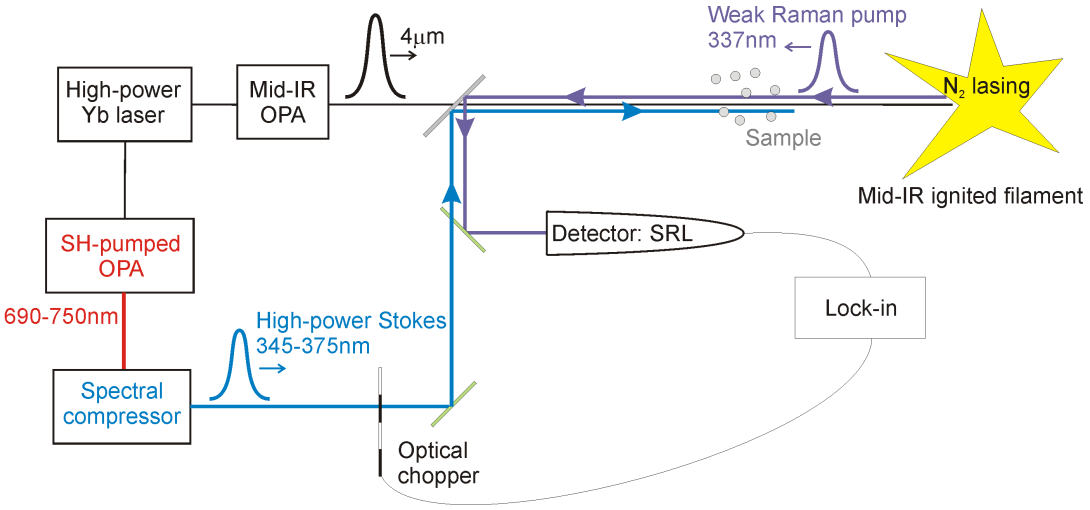

Fig. 9. *Architecture of the system for backward SRS experiment using as probe the atmospheric N_2 laser.*

The 4 μm OPCPA has been described in detail in the previous paragraph. Here we present the experimental setup for the tunable Stokes beam generation, shown in Fig. 10. We use the fourth harmonic of the uncompressed signal pulses of the OPCPA centered at 1460 nm. The spectrum of the signal wave extends from 1420 nm to 1520 nm, which gives a tunability of the fourth harmonics from 355 nm to 380 nm. This corresponds to a Raman shift with respect to the 337 nm radiation ranging from 1500 cm^{-1} to 3350 cm^{-1}. In order to boost the energy of the Stokes pulses a two stage OPA based on a 4-mm-thick type I BBO and a 10-mm-thick type I LBO crystal, pumped by a frequency-doubled fraction of the output of picosecond Nd:YAG laser system, was constructed. The OPA is seeded by the second harmonics of the OPCPA signal pulses which are spectrally filtered by using a 1700 nm transmission grating and 3-mm slit separated by a distance of 1.5 m. Due to the spectral filtering of the seed, the bandwidth of the amplified pulses is in the order of 1.5 nm FWHM, which after frequency doubling results in 0.7 nm FWHM UV Stokes pulses. Typical spectra of the output of the OPA and its second harmonics together with the 337 nm lasing from a filament are presented in Fig. 11, left panel. The two-stage OPA produces 0.9 mJ pulses which are frequency doubled in a 15 mm-thick BBO crystal. Energy of the generated UV pulses is in the order of 0.2 mJ while measurements of cross-correlation function with 200 fs pulses from the Yb:CaF2 CPA system reveal 7.4 ps pulse duration (Fig. 11, right panel).

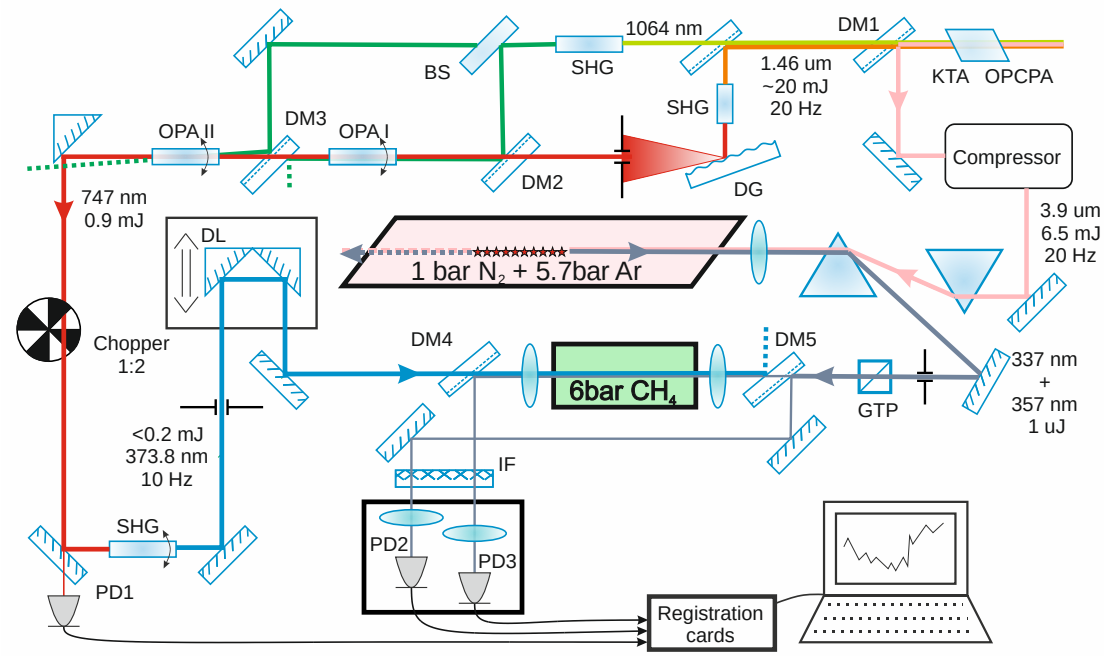

Fig. 10. *Scheme of backward SRS experiment using as probe the atmospheric N_2 laser. DL – delay line, DM – dichroic mirror, DG – diffraction grating, BS – beam splitter, IF – interference filter, PD – photodiode, GTP – Glan-Taylor polarizer.*

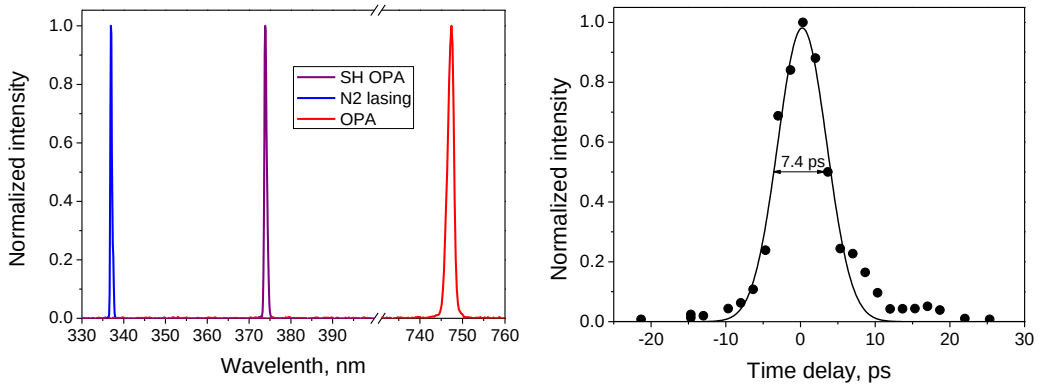

Fig. 11. *Left panel: spectra of the OPA (red line) and its second harmonic (violet line)together with the spectrum of the filament N_2 laser (blue line) . Right panel: cross-correlation of the UV pulse with a 200 fs IR pulse.*

One challenge of the setup is the spatial separation of forward propagating IR beam (the 4 μm filament igniter) and backward propagating UV light (the filament laser). Since it was difficult to identify suitable beam splitters, we decided to use a pair of CaF_2 Brewster prisms separated by a distance of 7 cm (Fig. 12). Because of the small distance between the prisms introduced for the 4-μm pulses, pulse spreading and spatial chirp effects are negligible. On the other hand, because of the different index of refraction for 4-μm (n = 1.40964) and 337-nm (n = 1.44814) light, back propagating UV pulses are deflected in such a way, that they bypass the apex of the second prism. Furthermore, because of the narrow bandwidth

of the backward propagating UV light an uncompensated divergence (angular chirp) after the propagating only through a single prism is negligible.

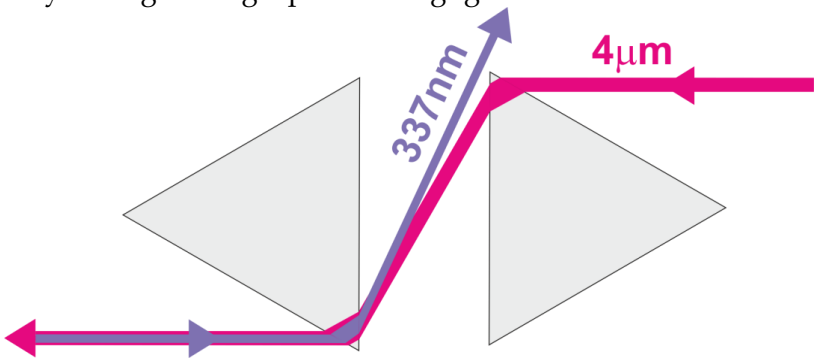

Fig. 12. *Brewster-prism-based dichroic beam splitter.*

Due to the low repetition rate of the laser system (20 Hz) and the energy fluctuations of the atmospheric laser, it was necessary to adopt a balanced scheme for the detection of the SRS signal. A part of the probe beam was reflected with a beam splitter (DM5 in Fig. 10) before the gas cell (reference beam), while the transmitted through the cell beam (probe beam) was picked by another dichroic mirror (DM4 in Fig. 10) which is transparent for the Stokes radiation. Both the reference and the probe pulses were sent into photodiodes PD2 and PD3 respectively, as shown in Fig. 10.

We have developed a setup allowing high precision measurement of the probe and reference pulse energies, according to the scheme proposed by Schriever *et al.* [17] and shown in Fig. 13. Two large area (33mm²) photodiodes with enhanced UV sensitivity down to 190nm (Hamamatsu model S1227-66 BQ) are used. The diodes are biased with a reverse voltage of 5 V. The photocurrent signal from the diode charges the capacitor C1 which is then discharged via the resistors R1 and R2 at a time constant of 22μs. C2 AC-couples the signal before it enters the operational amplifier (LT1220, chosen because of its low offset voltage and low bias current) and is subsequently amplified. The feedback loop contains a low pass filter. To screen the circuit from electromagnetic disturbances (e.g. from the Pockels cell on the same optical table), they were built into a metal box which was grounded. The power supply delivered most of the noise so it had to be replaced by batteries. At the diodes also filter were introduced (BNX00). Ceramic capacitors (100nF) were used at the circuit's power supply as well as at the operational amplifier's power supply. Larger capacitors (type electrolyte, slow) were introduced at the power supply at the circuit to make sure the voltage remains as constant as possible during the acquisition of the transient. The photodetector was tested to provide a linear response with incident light intensity up to an output voltage of 1.5V and the linearity between a pair of photodetectors was tested and the best ones were picked out of a set of 4 diodes. The 2kΩ potentiometer was adjusted in both diodes to the same signal shape.

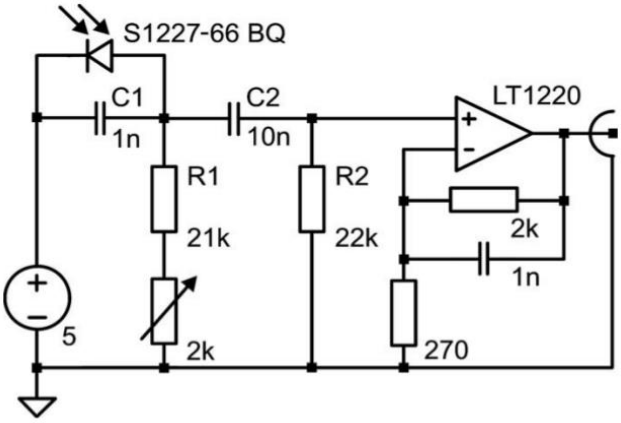

Fig. 13. *Scheme of the electronic circuit used for measuring the probe/reference energy.*

A high speed digitizer from National Instruments (PCI 5122, 14bit, 2 channel, 50 Ohm terminated) was taken to record the probe and reference signals simultaneously. The transients were sampled, filtered (Bessel) and then reduced to a single value by taking the difference of the zero signal shortly before the onset of the transient and the transient itself. The best choice was to take an integral value for the transient out of the first part of the falling slope whereas the peak value delivered not as good probe/reference correlations.

For the pump-probe setup also the energy of the pump beam had to be registered, for which we used a simple E-series card from National Instruments, synchronized to the PCI 5122. Due to slow fluctuation of the output energy of the picosecond Nd:YAG laser (with the periodicity of a few seconds) only consecutive pump-on pump-off shots were allowed. After that check a cross correlation was calculated and only those measurements pairs which exceeded a certain threshold (in this particular case it was 0.95) were taken to further increase accuracy by excluding laser signal which were biased too much by noise. Another check was performed on a signal threshold level which was set to 200mV peak-to-peak value. A photograph of the backward SRS setup using as a probe the N_2 filament laser is reported in Fig. 14.

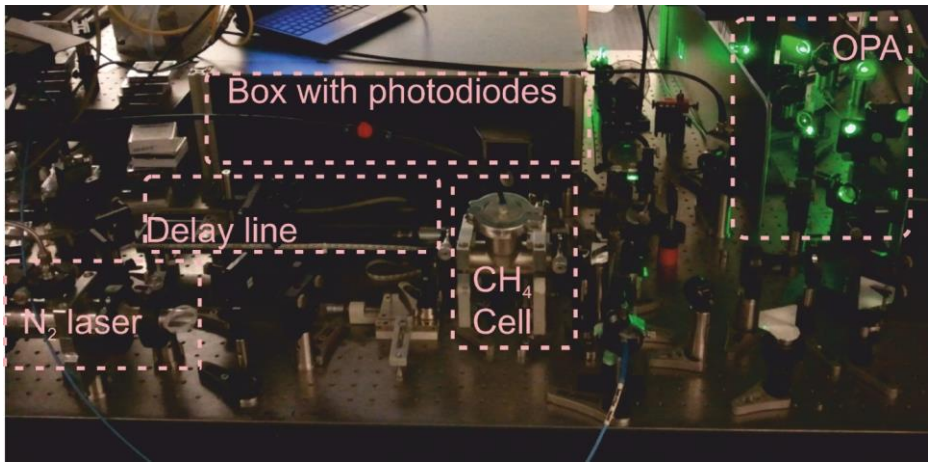

Fig. 14. *Picture of the experimental setup for backward SRS from an atmospheric laser.*

6_ Experimental demonstration of Stand-off SRS with a filament laser

In order to detect the backward SRS signal it is necessary to provide spatial, temporal and spectral (corresponding to the Raman shift of the molecule under investigation) overlaps. Spatial overlap was implemented by matching the pump and Stokes beams with a help of a diaphragm. Finer adjustment of the spatial overlap was made by maximizing the magnitude of the signal. Both pump and Stokes beams were focused with 10-cm focal length lenses resulting in waist radii of w_{probe} = 35 μm and w_{pump} = 50 μm and Rayleigh ranges of z_{probe} = 2.9 mm and z_{pump} = 5.5 mm, as measured with a beam-profiler (Fig. 15). The waists of the pump and Stokes beams are not matched, first, because of the different beam diameters on the focusing lenses and, second, because of the different beam quality parameters M^2. We have determined beam quality parameters for the Stokes and pump beams to be M^2= 8 and M^2= 10 respectively. To our knowledge, this is the first evaluation of the beam quality of a filament-assisted N_2 laser.

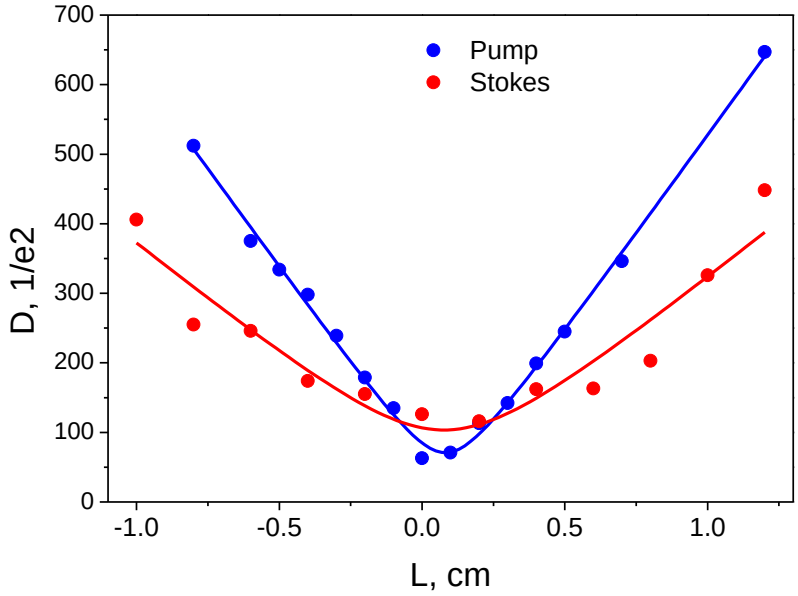

Fig 15. *The waists of the pump and Stokes beams after focusing with 10-cm focal length lens as determined with a beam profiler.*

In order to determine the temporal overlap between the pump and Stokes pulses, we performed a pump-probe experiment using a sample of the Coumarin500 laser dye. The dye was chosen because: 1) it has strong photoinduced absorption in a broad wavelength range; 2) it has excited state lifetime of several nanoseconds; 3) it has strong ground state absorption in the vicinity of 370 nm, where the strong Stokes pulses are centered and is

practically transparent around 337 nm, where the Raman pump pulses, acting as a probe in the SRL experiment, are situated. For the determination of the temporal overlap a 1 mm-thick quartz cell containing ethyl-alcohol solution of Coumarin500 dye was placed in the spatial overlap region of the pump and Stokes beams. Figure 16 shows the pump-probe signal in Coumarin500 as a function of the pump-probe delay. The measurements in Coumarin500 allowed us to determine the exact time zero between pump and Stokes pulses as well as to optimize the spatial overlap of the beams.

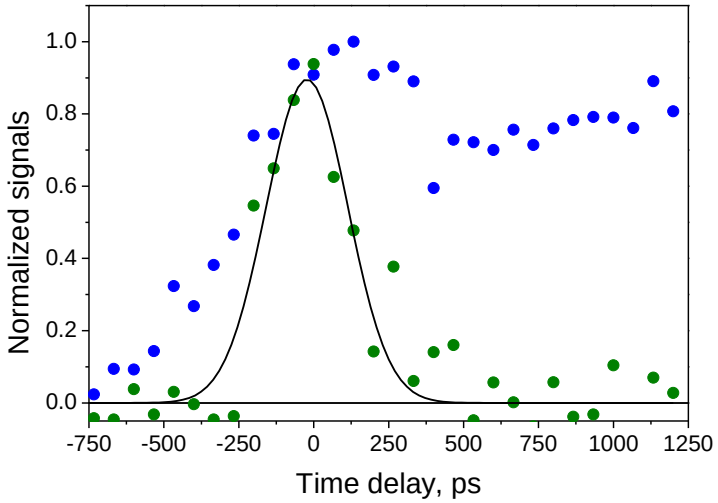

Fig 16. ***T****ime delay dependence of the photoinduced absorption in Coumarin500 probed at 337 nm while pumping at 374 nm (blue dots), compared to the SRL in* CH_4 *(olive dots). A Gaussian fit to the SRL data is given by a solid black line.*

Next, in order to detect SRL in CH_4, the pump-Stokes frequency detuning had to be adjusted to match the 2917 cm^{-1} ν_1 band. The nitrogen laser emits at 337 nm and its bandwidth was determined to be <2 cm^{-1} by a single Czerny-Turner monochromator. The OPA wavelength was tuned to 748 nm, with the corresponding second harmonic centred at 374 nm. The spectral width of the Stokes pulses was measured to be 0.7 nm (~50 cm^{-1}) FWHM, using a spectrometer with 0.3 nm resolution (USB 2000, Ocean Optics). The rather broad bandwidth of the Stokes pulses is determined by the limited spectral selectivity of the diffraction grating based filter described in the previous section. Spectra of pump and Stokes pulse are reported in Fig. 17.

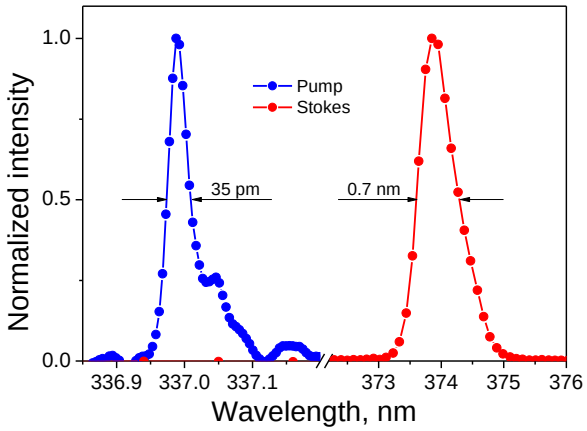

Fig 17. *Spectra of pump and Stokes pulses.*

Having set the proper detuning between pump and Stokes pulses, we recorded the SRL signal in a gas cell filled with 6 bar of CH_4. The maximum SRL signal was measured to be 6×10^{-3}, which is a factor of 3 higher than in the preliminary experiments reported in Section 3. By changing the pump-Stokes delay, as shown in Fig. 18, we are now in a position to determine the duration of the N_2 filament laser pulse, which was found to be 360 ps. For a filament N_2 laser the pulse length is determined by either the lifetime of the excited N_2 (in the case of a very short filament) or by both the lifetime and the length of a filament (if the length of a filament is close to or longer than a product of the pulse duration and the speed of light). In our particular conditions, the 360 ps pulse duration is consistent with a filament length, determined visually, between 10 and 20 cm.

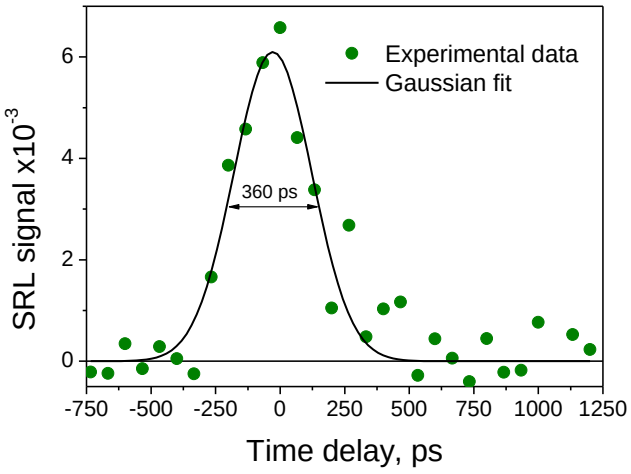

Fig 18. *Dependence of SRL signal in CH_4 (6 bars pressure) on the delay between the Stokes and pump pulses. Dots are experimental data accumulated over 1000 successful shots. Black solid line is Gaussian fit to the experimental data.*

The dependence of the SRL signal on pump-Stokes frequency detuning was characterized in Fig. 19 by simultaneously tuning the OPA and the second harmonic

crystals. As expected the measured spectrum peaks at around 2915 cm^{-1}. The bandwidth of the measured response is in the order of 0.5 nm and is determined by the spectral width of the Stokes pulse. In order to verify that the measured SRL signal is not influenced by the variation of the pulse energy during OPA tuning, in parallel we have recorded a pump-probe signal in Coumarin500 and observed a nearly constant signal upon Stokes pulse tuning.

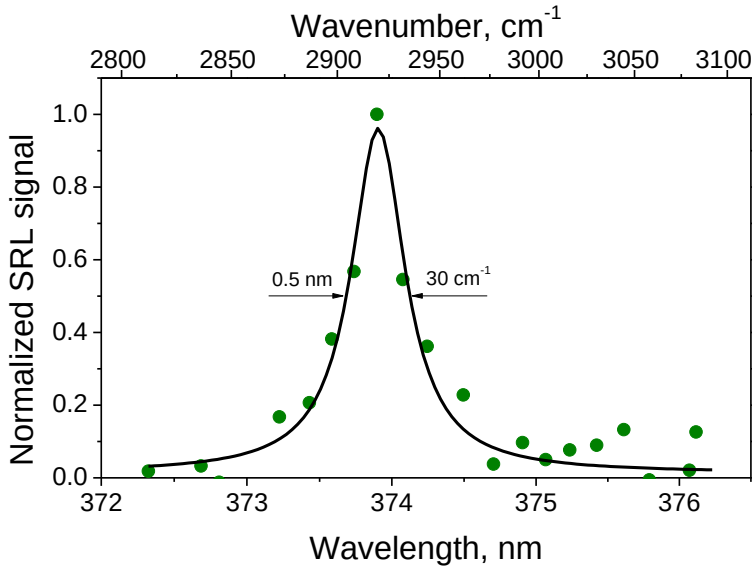

Fig 19. *SRL spectrum measured in CH_4 at 6 bar pressure; dots represent experimental points obtained by averaging over 2000 successful shots. Black solid line is the result of fitting with a Lorentzian function.*

In order to determine the sensitivity of our apparatus, we have recorded the SRL signal as a function of CH_4 pressure (Fig. 20). The measurement revealed a linear concentration dependence that is characteristic of SRS. From the figure it can also be seen that the lowest detectable pressure at the present conditions is in the order of 1 bar, indicating that, for realistic detection of atmospheric contaminants, the sensitivity should be substantially improved. One way to improve sensitivity is a substantial increase of Stokes pulse energy. For this, one needs to build a different type of OPA, which is based on narrowband seed amplification (possibly of parametric superfluorescence) while keeping the amplified pulse duration close to that of the driving laser (70 ps). For this type of parametric amplifier a set of large aperture nonlinear optical crystals (for example DKDP) is needed.

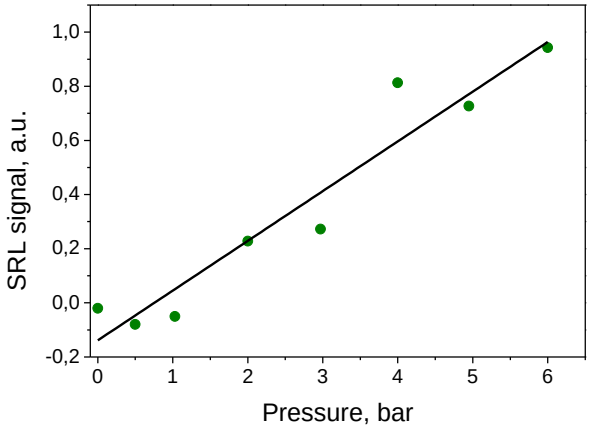

Fig 20. *SRL spectrum measured in CH_4 at 6 bar pressure; dots represent experimental points obtained by averaging over 2000 successful shots. Black solid line is the result of fitting with a Lorentzian function.*

7_ Improving the filament laser: pulse shaping at 3 micron

In order to optimize the filament dynamics and the population inversion leading to N_2 lasing, with the ultimate goal to reach the holy grail of laser action in the atmosphere in the absence of Ar, it is important to perform pulse shaping of the mid-IR driving pulse. This represents a great technical challenge because the techniques of direct spectral phase shaping in the mid-IR are in their infancy and their average power and pulse energy handling capabilities are very poor. To meet this challenge, UHEI in the last year of the project was able to acquire a state-of-the-art mid-IR pulse shaping system based on a Germanium acousto-optic modulator (AOM). In cooperation with POLIMI, the two groups are exploring direct broadband mid-IR shaping around the wavelength of 3 μm.

The broadband mid-IR OPA developed for this purpose is based on a design previously reported by POLIMI [18]. There are several nonlinear crystals with extended IR transparency which, when pumped at 0.8 μm, display a broad phase-matching bandwidth for parametric amplification around 1 μm, allowing for the direct generation of broadband idler pulses with spectra spanning the 3–5 μm wavelength range and supporting a two optical-cycle transform-limited (TL) duration.

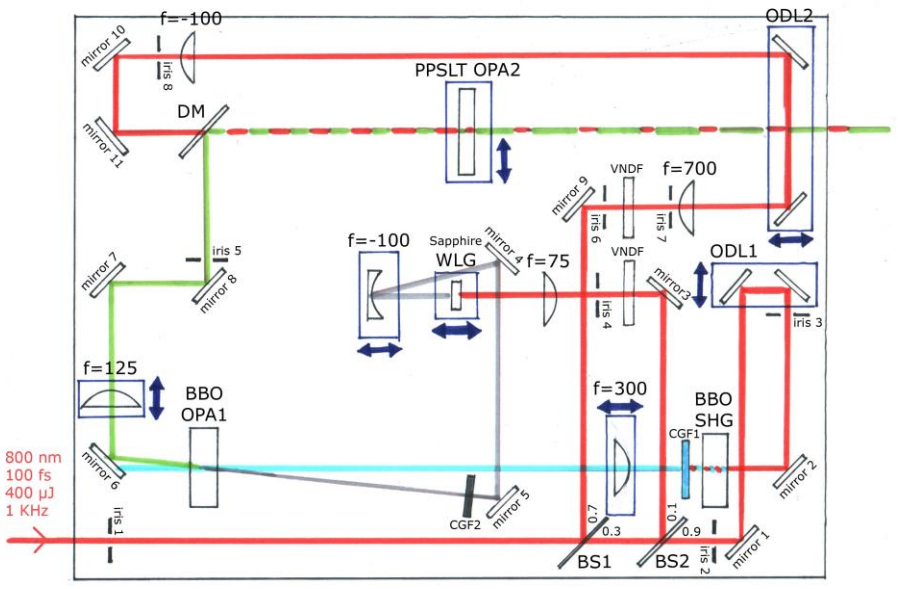

Fig. 21. *Scheme of the broadband mid-IR OPA.*

The experimental setup of the two-stage OPA is shown in Fig. 21. It is pumped by 400 μJ, 100 fs, 800 nm, 1 kHz pulses from a Ti:sapphire laser / regenerative amplifiersystem (Coherent Libra). A few μJ fraction of the laser output is focused in a 2-mm-thick sapphire plate to generate a single-filament white light continuum used as the seed of the first stage. The first OPA stage is pumped by the second harmonic (400 nm) and uses a BBO crystal ($\theta = 29°$) to amplify the near-IR part of the continuum around 1 μm. The first stage produces ≈1 μJ signal pulses, which are spatially filtered from pump and idler thanks to the slightly non-collinear geometry. The amplified signal and the second pump are then combined by an 850 nm edge dichroic beam splitter and sent to the second

stage, which uses a strictly collinear geometry to avoid angular dispersion of the broadband idler beam. The second stage amplifies the signal up to 8 μJ and generates mid-IR idler pulses, optimized for the broadest spectrum, with ≈2 μJ energy. The use of a two-stage configuration offers several advantages, such as (i) the possibility to drive the second OPA stage more easily into saturation, with improved conversion efficiency and remarkable stability of the idler (1% rms energy fluctuations); (ii) better control of the collinearity between the signal and pump beams in the second OPA stage, thus avoiding any angular dispersion of the idler.

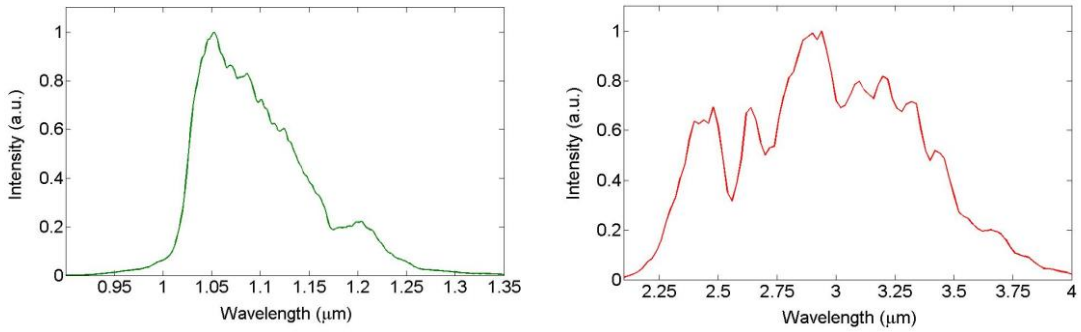

Fig. 22. *Typical spectra of the signal (left panel) and idler (right panel) pulses generated by the OPA.*

A typical spectrum of the broadband mid-IR OPA is shown in Fig. 22 for both the signal (left panel) and the idler (right panel). As it can be seen, the idler spectrum extends over nearly one octave and supports a TL pulse duration of approximately 15 fs. A photograph of the mid-IR OPA is shown in Fig. 23.

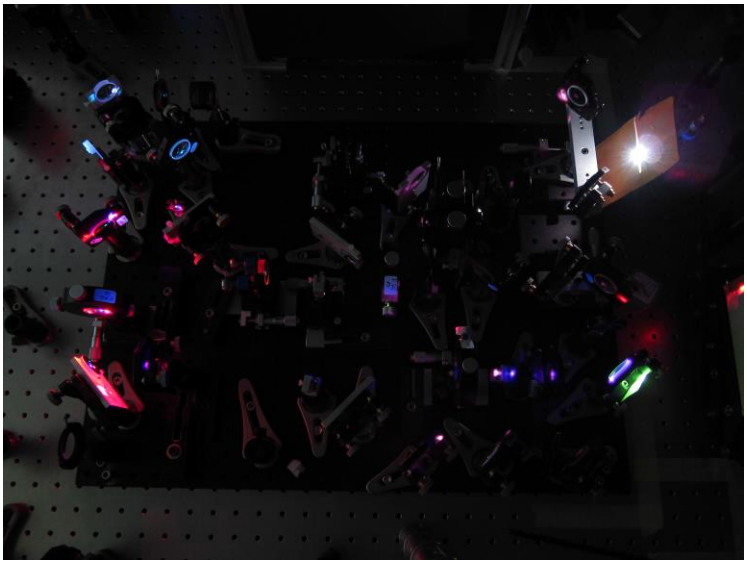

Fig. 23. *Photograph of the broadband mid-IR OPA.*

The OPA was then transferred to UHEI, where it was coupled to the broadband AOM-based mid-IR pulse shaper, according to the setup shown in Fig. 24.

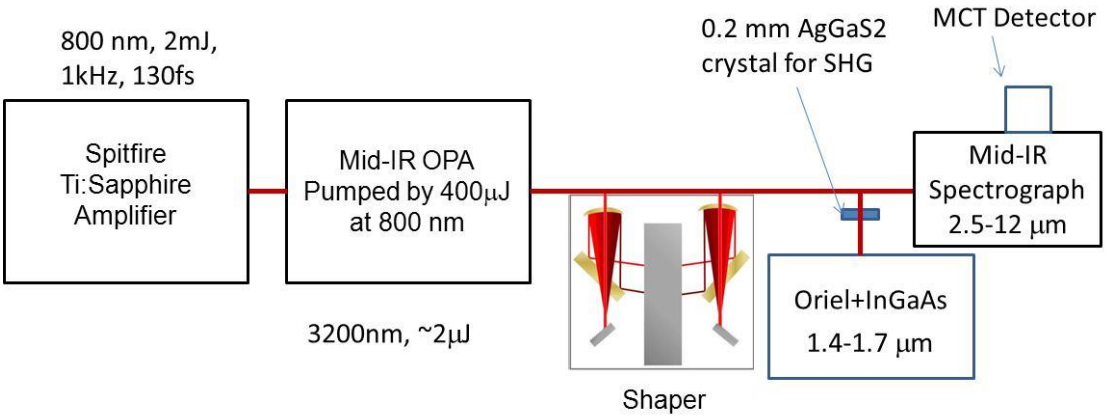

Fig. 24. *Typical spectra of the signal (left panel) and idler (right panel) pulses generated by the OPA.*

The shaper is based on the design proposed by Warren and co-workers[19], and extended by Zanni *et al.* to the mid-IR range [20]. The OPA pulses are dispersed on a 150 gr/mm grating with λ_{blaze}=8.6μm oriented for the 3th order and collimated with an f=170mm cylindrical mirror, creating a cylindrical spot in the Fourier plane in the shaper (see Fig. 25). The Ge AOM (Isomet LS600-1109-10W) is placed in the Fourier plane. A computer controlled arbitrary waveform generator create an acoustic wave with a 75MHz center frequency that propagates along the length of Ge crystal at 5,5 mm/μs. The crystal size of 55mm gives a time aperture of 10μs. Since the speed of a sound wave in Ge is approximately four orders of magnitude slower than the speed of light, the acoustic wave acts like a transmission grating, deflecting the frequencies of interest in the first order with programmable amplitude and phase. After the AOM the diffracted light is recombined in the second part of the 4f setup. The overall efficiency of the total shaper system is more than 50%. For our design we estimated around 500 resolvable elements across the crystal aperture. Unfortunately, due to the present unavailability of gratings blazed for 3 μm, we had to resort on the 3rd order diffraction of the available gratings, which severely limited the acceptance bandwidth of the shaper, as shown in Fig. 26, left panel. It was therefore only possible presently to transmit through the shaper pulses with a bandwidth corresponding to a 60-fs TL duration. By acquiring proper gratings, it should be possible to handle the full 15-fs pulse bandwidth. Since the Ge AOM crystal is 2cm thick, it introduces huge high order spectral phase dispersion. To some extent the compensation of the second-order dispersion from Ge can be performed by translating the output grating and at the same time monitoring the SHG signal of Mid-IR pulse. The shaper can be used for fine compensation of the higher order spectral phase dispersion. By recording a SHG-FROG map of the mid-IR pulses using a 0.2 mm $AgGaS_2$ crystal, we could retrieve a pulse duration of 95 fs, which is close to the 60 fs TL value. This demonstrates successful coupling of the broadband mid-IR pulse to the AOM-based shaper. By using proper gratings able to handle the whole pulse

bandwidth, we will be able to perform shaping of a few-optical-cycle mid-IR pulse. The know-how will then be transferred to UNIWIE for shaping of the mid-IR pulse driving the filament laser.

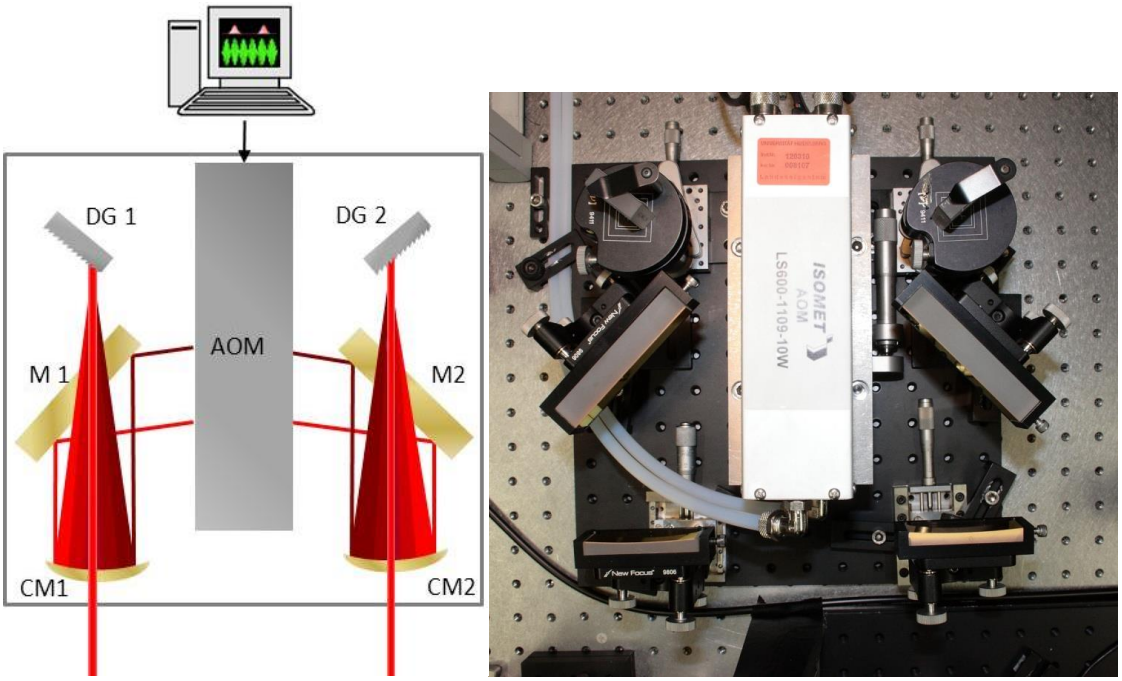

Fig. 25. *Left panel: conceptual scheme of the mid-infrared pulse shaper based on a Ge acousto-optic modulator (AOM). DG1, DG2: diffraction grating; M1, M2: plane mirrors; CM1, CM2: curved mirrors. Right panel: photograph of the experimental setup.*

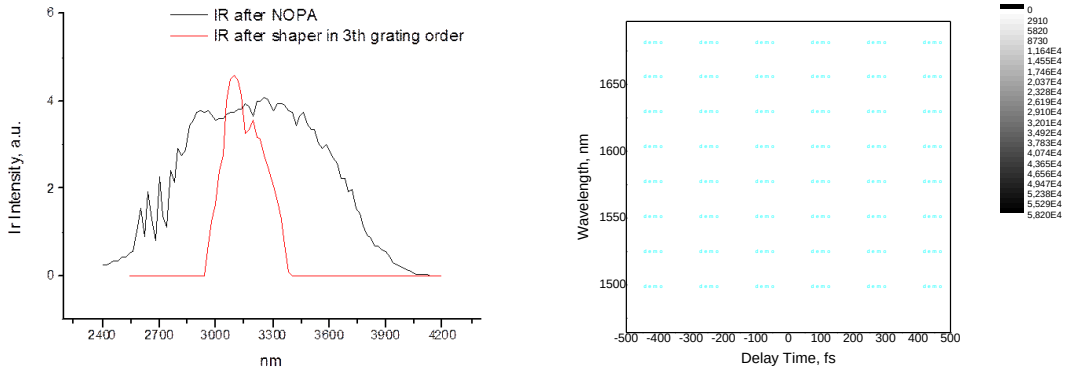

Fig. 26. *Left panel: spectra of the mid-IR OPA before (black line) and after (red line) the shaper. Right panel: SHG-FROG trace of the compressed mid-IR pulses after the shaper.*

8 CONCLUSIONS

In this deliverable:

- we identified backward SRS as a suitable technique for coherent standoff sensing;
- performed preliminary experiments aimed at identifying the parameters for standoff backward SRS;
- we demonstrated a backward propagating filament assisted N_2 laser, which is the cornerstone for any coherent standoff detection scheme;
- we designed and developed a system for backward SRS using as a probe an N_2 filament laser;
- we experimentally demonstrated backward SRS using an atmospheric filament as a probe; this can be considered as the main result of the CROSSTRAP project;
- we implemented a system for shaping broadband mid-IR pulses, aimed at optimizing the performance and the efficiency of the filament laser.

9 REFERENCES

1. A.P. Cracknell and L. Hayes, *Introduction to remote sensing* (Taylor & Francis, London, 2006).
2. C. Weitkamp, ed., *Range-resolved optical remote sensing of the Atmosphere* (Springer, Berlin, 2005).
3. G. Turrell and J. Corset, *Raman microscopy: developments and applications* (Academic Press: San Diego, CA, 1996).
4. J. Kasparian and J.-P. Wolf, "A new transient SRS analysis method of aerosols and application to a nonlinear femtosecond lidar," Opt. Commun. **152**, 355 – 360 (1998).
5. O. Katz, A. Natan, Y. Silberberg, and S. Rosenwaks, "Standoff detection of trace amounts of solids by nonlinear Raman spectroscopy using shaped femtosecond pulses," Appl. Phys. Lett. **92**, 171116 (2008).
6. H. Li, D.A. Harris, B. Xu, P.J. Wrzesinski, V.V. Lozovoy, and M. Dantus, "Standoff and arms-length detection of chemicals with single-beam coherent anti-Stokes Raman scattering," Appl. Opt. **48**, B17-B22 (2009).
7. P.R. Hemmer, R.B. Miles, P. Polynkin, T. Siebert, A.V. Sokolov, P. Sprangle, and M.O. Scully, "Standoff spectroscopy via remote generation of a backward-propagating laser beam," Proc. Natl. Acad. Sci. USA **108**, 3130-3134 (2011).
8. Y. V. Rostovtsev, Z.-E. Sariyanni, and M. O. Scully, "Electromagnetically induced coherent backscattering," Phys. Rev. Lett. **97**, 113001 (2006).
9. L. Yuan, K.E. Dorfman, A.M. Zheltikov, and M.O. Scully, "Plasma-assisted coherent backscattering for standoff spectroscopy," Opt. Lett. **37**, 987-989 (2012).
10. A.M. Zheltikov, M.N. Shneider, and R.B. Miles, "Radar return enhanced by a grating of species-selective multiphoton ionization as a probe for trace impurities in the atmosphere," Appl. Phys. B **83**, 149 - 153 (2006).
11. A. Dogariu, J.B. Michael, M.O. Scully, and R.B. Miles, "High-gain backward lasing in air," Science **331**, 442–445 (2011).
12. D. Kartashov, S. Alisauskas, G. Andriukaitis, A. Pugzlys, M. Shneider, A. Zheltikov, S.L. Chin and A Baltuska, "Free-space nitrogen gas laser driven by a femtosecond filament", Phys. Rev A. **86**, 033831 (2012).
13. E. Ploetz, S. Laimgruber, S. Berner, W. Zinth, and P. Gilch "Femtosecond stimulated Raman microscopy," Appl. Phys. B **87**, 389–393 (2007).
14. Ch. W. Freudiger, W. Min, B. G. Saar, S. Lu, G. R. Holtom, C. He, J. C. Tsai, J. X. Kang, and S. X. Xie, "Label-free biomedical imaging with high sensitivity by stimulated Raman scattering microscopy," Science **322**, 1857-1861 (2008).
15. P. N. Malevich, D. Kartashov, Z. Pu, S. Ališauskas, A. Pugžlys, A. Baltuška, L. Giniūnas, R. Danielius, A. A. Lanin, A. M. Zheltikov, M. Marangoni, and G. Cerullo, "Ultrafast-laser-induced backward stimulated Raman scattering for tracing atmospheric gases," Opt. Express **20**, 18784-18794 (2012).
16. G. Andriukaitis, T. Balčiūnas, S. Ališauskas, A. Pugžlys, A. Baltuška, T. Popmintchev, M.-C. Chen, M.M. Murnane, and H.C. Kapteyn, "90 GW peak power few-cycle mid-infrared pulses from an optical parametric amplifier," Opt. Lett. **36**, 2755-2757 (2011).
17. C. Schriever, S. Lochbrunner, E. Riedle and D. J. Nesbitt "Ultrasensitive ultraviolet-visible 20 fs absorption spectroscopy of low vapor pressure molecules in the gas phase", Rev. Sci. Instrum. **79**, 013107 (2008).

18. D. Brida, M. Marangoni, C. Manzoni, S. De Silvestri, and G. Cerullo, "Two-optical-cycle pulses in the mid-infrared from an optical parametric amplifier," Opt. Lett. **33**, 2901-2903 (2008).
19. M.A. Dugan, J.X. Tull, and W.S. Warren, "High-resolution acousto-optic shaping of unamplified and amplified femtosecond laser pulses", J. Opt. Soc. Am. B **14**, 2348-2358 (1997).
20. S.-H. Shim, D.B. Strasfeld, E.C. Fulmer, and M.T. Zanni, "Femtosecond pulse shaping directly in the mid-IR using acousto-optic modulation," Opt. Lett. **31**, 838-840 (2006).